JACS
JOURNAL OF THE AMERICAN CHEMICAL SOCIETY
pubs.acs.org/JACS
Article

Elevating Nitrate Reduction through the Mastery of Hierarchical Hydrogen-Bond Networks

Ru-Yu Zhou,[#] Shisheng Zheng,[#] Xuan Liu, Yao-Hui Wang, Shunning Li, Xinzhe Yang, Feng Pan,* and Jian-Feng Li*

Cite This: J. Am. Chem. Soc. 2025, 147, 20504−20511
Read Online
ACCESS | Metrics & More | Article Recommendations | Supporting Information

ABSTRACT: To effectively resolve environmental and industrial dilemmas, electrochemical reduction of nitrate (NO_3^-) to ammonia (NH_3) offers a brilliant strategy for tackling pollution and creating economic value, but the scarcity and reduced reactivity of available interfacial water and reactive adsorbates represent ongoing obstacles. Here, we reform the water−ion networks via electrolyte concentration manipulation and electrode construction on atomically flat Au single-crystal surfaces. With the combination of in situ Raman spectroscopy and multifidelity theoretical simulations, we pinpoint H_2O with dual hydrogen-bond donors as an observable indicator for nitrate electroreduction (NO_3RR). A hierarchical configuration characterized by structured Li^+·NO_3^- planes coupled with enriched hydrogen-bond networks is verified to streamline the reactive intermediates activation and proton transport, thus synergistically boosting NO_3RR. We highlight the cooperative modulation of the interfacial water−ion interactions and the hydrogen-bond networks in optimizing NO_3RR. Our findings unveil microscale viewpoint of synergy between the local ion−water interactions and connectivity of the hydrogen-bonding network.

INTRODUCTION

As a vanguard of green energy and a pillar of sustainable agriculture, ammonia (NH_3) stimulates continuous progress in farming, plastics, and chemical industries, epitomizing the intersection where sustainable oversight harmonizes with productive industry.[1] The electrochemical reduction of nitrate (NO_3^-) promises not only to reinvent sustainable fabrication techniques but also to address the problem of NO_3^- pollution, which compromises aquatic ecosystems and challenges global nitrogen cycle.[2] In the realm of nitrate reduction reaction (NO_3RR), a delicate balance must be reached and it requires precise modulation to ensure it donates adequate protons for the hydrogenation reaction, meanwhile avoiding engagement in the undesired hydrogen evolution reaction (HER).[3] This subtle control over the role of interfacial water is pivotal for optimizing the efficiency and selectivity of the NO_3RR.[4]

To decode the mechanism of interfacial electrocatalytic reactions, comprehensive insight into the microstructure structure of the solid−liquid interface is imperative. The evolving electric double layer (EDL) structure inspires accurate depictions of the configuration and connectivity of interfacial hydrogen-bond networks and water−ion networks under bias potentials.[5,6] The intricate hydrogen-bond networks at interfaces serve as the underlying microscopic origin for the kinetics of electrochemical processes, profoundly impacting the energy conversion efficiency. Ions induce significant perturbation to the hydrogen-bond network of interfacial water, critically shaping the characteristics of EDLs. On the one hand, the molecular insights into the dynamics of an electrocatalytic process are rooted in the organization of water−ion networks at the interface.[7] Notably, the water−ion interactions can directly facilitate the activation of reactive species and initiate the reaction, as elucidated in previous work that accumulation of cations at the interface can induce ordered interfacial water structures and accelerate the water dissociation.[8] On the other hand, the hydrogen-bond network of interfacial water plays a vital role in proton transfer, a well-recognized key factor influencing the sustainability of the reaction.[9] Significantly, these two aspects should be intertwined, like two sides of the same coin, particularly in complex multielectron proton-coupled electrochemical reactions.

In tandem with recognition of the indispensability of high-performance catalysts of the NO_3RR, knowledge deficits still exist regarding active phases and reaction kinetics at reconstructed surfaces. Considering the profound impact of the solid−electrolyte interface takes center stage, the properties of electrolyte encompassing cations, anions, H_2O content, electrolyte concentration, and pH significantly govern the kinetics of electrocatalytic NO_3RR.[10,11] Although precise

Received: February 13, 2025
Revised: May 30, 2025
Accepted: June 2, 2025
Published: June 7, 2025

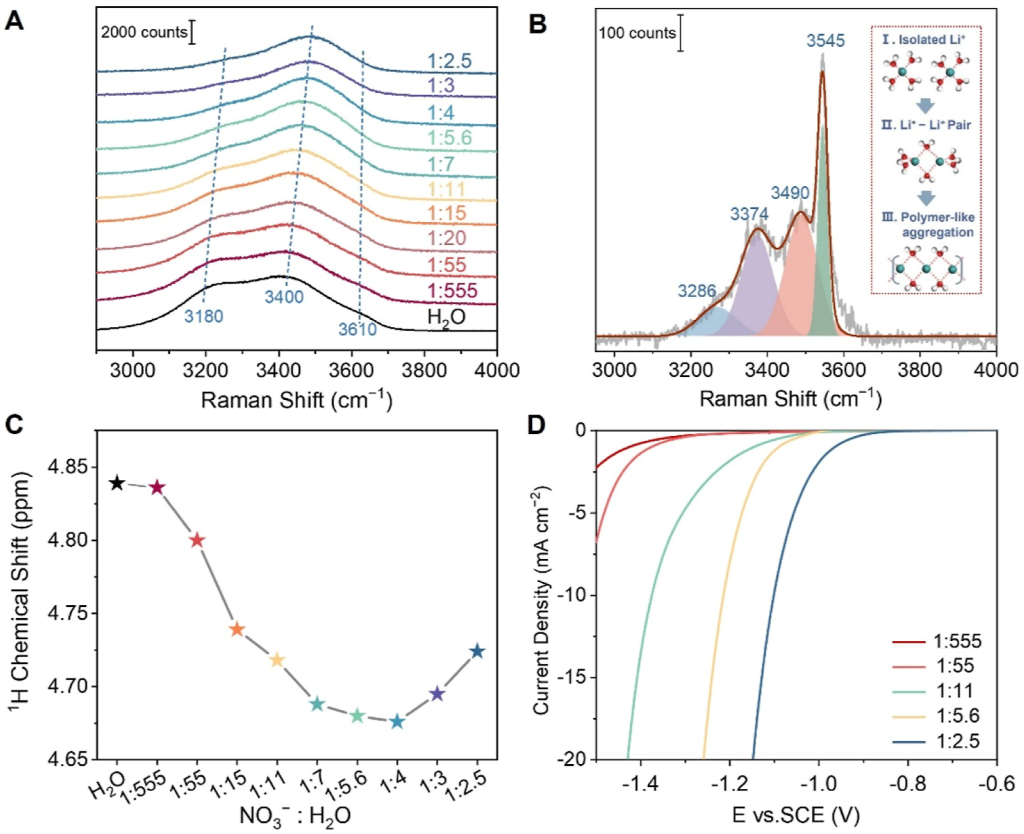

Figure 1. Solvation structures of $LiNO_3$ solutions. (A) O−H stretching band of bulk $LiNO_3$ solutions and pure water. (B) The O−H stretching vibration of Li·xH_2O and schematic diagram of Li−H_2O interaction state with varying $LiNO_3$ concentrations. (C) Chemical shifts for H nuclei in $LiNO_3$ solutions. (D) LSV of Au(111) in $LiNO_3$ solutions.

engineering of the local interfacial architecture for optimized nitrate electroreduction is paramount, the intricate details regarding how ions and interfacial water affect the NO_3RR to yield NH_3 remain enigmatic, presenting a formidable conundrum for experimental practitioners aiming to discern suitable electrolyte compositions. Real-time description of hydrogen-bond networks, distribution, and interactions of ions are essential yet hard to achieve, especially at extreme potentials and high concentrations. Considerable theoretical and experimental efforts have been devoted to achieving a microscopic understanding of ion solvation and hydrogen-bond environments of water−ion networks. The characteristics of the cations, such as size and the hydration, have a significant effect on various electrochemical reactions.[12,13] Anions in the electrolyte modulate microenvironments proximal to the catalyst surface and affect product distribution, especially when particularly when they serve as primary reactants in interfacial processes such as the electroreduction of NO_3^- and the formation of a solid electrolyte interface (SEI) in alkali-metal-ion batteries.[14] Recent investigations have unveiled that anions actively engage in the interfacial hydrogen-bond networks, with their decomposition notably promoted in high concentration electrolytes.[15] Despite significant advancements, the precise architecture of anions, their interplay with cations and water at interfaces, and their fundamental function in governing interfacial reactivity remain enigmatic, remaining a topic of ongoing doubt.

Daunting questions for experimental investigation of the EDL structure principally lie in the intricate interplay of interactions and the dynamic evolution of water−ion networks.[16] However, harsh electrochemical conditions complicate the understanding of interfacial dynamics due to complex water−ion interactions and hydrogen-bond fluctuations. As an advanced analytical technique with exceptional surface sensitivity, shell-isolated nanoparticle-enhanced Raman spectroscopy (SHINERS) overcomes the material and morphological limitations of conventional surface-enhanced Raman spectroscopy (SERS) and effectively utilized to decipher EDL configurations under specialized scenarios.[17,18] In this article, we delve into the interfacial water structure and the reduction dynamics of anions in $LiNO_3$ aqueous electrolytes across varying concentrations on atomically ordered and stable Au single-crystal surfaces by combining in situ SHINERS and multifidelity molecular dynamic (MD) simulation. Au single-crystal surfaces were selected as an ideal platform for probing the structure−activity correlation between interfacial water−ion network dynamics and NO_3RR activity, leveraging their optimal NO_2^- adsorption, and inherent suppression of competing hydrogen evolution, which collectively govern selective NH_3 formation. Specifically, we note that the ordered $Li^+{\cdot}NO_3^-$ planes, with NO_3^- lying flat against the electrode surface, promotes the activation of adsorbed NO_3^- under high electrolyte concentrations. Moreover, the hydrogen bonds formed between out-plane NO_3^- and H_2O significantly enrich hydrogen-bond networks at the interface and further accelerate NO_3RR. Notably, through modulating the crystallographic orientation and electronic structure of the electrode, the NO_3RR was further enhanced by rational constructing the interfacial water−ion networks. Our findings suggest that strategically modulating water−ion interactions and the

https://doi.org/10.1021/jacs.5c02540
J. Am. Chem. Soc. 2025, 147, 20504−20511

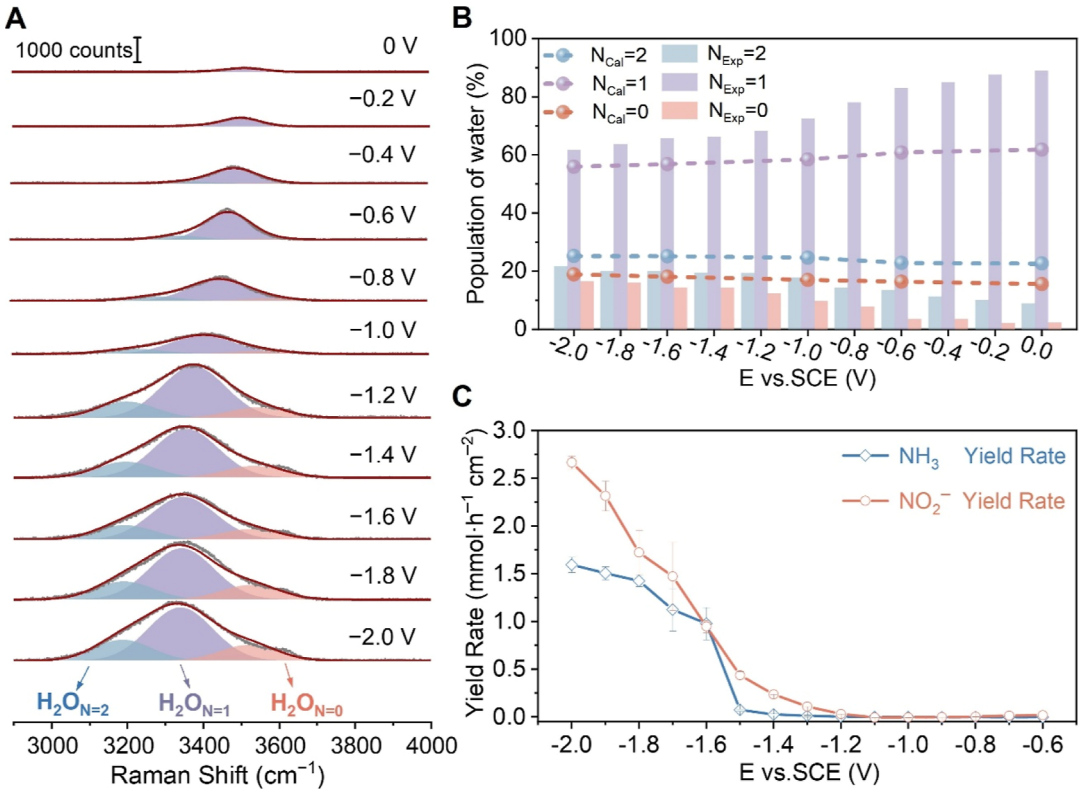

Figure 2. Probing the 1:11 Au(111)/$LiNO_3$ interface. (A) In situ Raman spectra of the O−H stretching mode of interfacial H_2O (gray curves). Gaussian fits of H_2O with 2, 1, and 0 donors are shown in blue, purple, and red, respectively. (B) Potential-dependent population of interfacial H_2O. The experimental and simulated results are presented by columns and dashed lines, respectively. (C) Potential-dependent ammonia (blue) and nitrite (orange) yield rate.

connectivity of hydrogen-bond networks is a groundbreaking approach to engineer the intricate landscapes of interfacial water environments.

RESULTS AND DISCUSSION

Solvation Structure of $LiNO_3$ Solutions. The $LiNO_3$ solutions across a wide range of molar ratios of $LiNO_3$ to H_2O (1:555 to 1:2.5) were characterized by Raman spectroscopy, as shown in Figures 1A and S3. As the concentration of $LiNO_3$ increases, the structure of water in the solution undergoes significant changes and the O−H vibration modes of water molecules, which are highly sensitive to the organization of water and intermolecular interactions, provide valuable insight into this transition. As the concentration increases, the width of the O−H stretching vibration peak progressively narrows, accompanied by a decrease in its intensity, indicating the formation of more structured water networks. Additionally, the blue-shift of the O−H stretching vibration suggests a strengthening of the O−H bond, implying a higher energy requirement for bond disruption and a weakening of the hydrogen-bond network. The Raman profile of the hydrate crystal Li·xH_2O is shown in Figure S4 and its O−H band deconvolved into four components (Figure 1B), specifically, 3286 cm^{-1}, 3374 cm^{-1}, 3490 cm^{-1}, and 3545 cm^{-1}. These spectral features are indicative of a polymer-like chain, which is enveloped by nitrate ions through electrostatic interactions. This crystal structure forms a critical foundation for deducing the arrangement in superconcentrated $LiNO_3$ solutions.[19] The structure of this crystal serves as a significant basis for inferring the structure of superconcentrated $LiNO_3$ solution. The Raman data demonstrate the transition of the water molecule structure from isolated units to clusters, ultimately forming a polymer-like chain, as visualized in the inset scheme in Figure 1B.

The concentration dependence of the chemical shift, observed through proton nuclear magnetic resonance (^1H NMR) spectroscopy at varying $LiNO_3$ concentrations, is illustrated in Supporting Information Figure S5 and their ^1H chemical shift are shown in Figure 1C. From 1:555 to 1:4, the ^1H signal of water molecules progressively shifts from 4.84 to 4.68 ppm. This shift is attributed to a decrease in electron density near the protons, resulting from amplified long-distance interactions between water molecules, signaling the formation of larger water networks. Intriguingly, at higher concentrations, the ^1H signal shifts further upfield, indicating a reduction in hydrogen bond density and an increase in Li^+-O_H (water oxygen) interactions. To further correlate the water structure with electrochemical activity, steady-state polarization curves were recorded and are presented in Figure 1D. As the concentration increases, the onset potential of the overall reduction reaction shifts positively, indicating enhanced interfacial reduction activity. These findings suggest that the dominant mechanism governing the interfacial activity extends beyond the influence of ion−water interactions in bulk solutions. Instead, the critical role of the water network at the interface warrants further investigation.

In Situ Probing of the EDL Structures. Electrochemical SHINERS were employed to probe the EDL structures on Au(*hkl*) in $LiNO_3$ electrolytes, donoted as Au(*hkl*)/$LiNO_3$, across a range of concentrations (1:555 to 1:2.5), with detailed

https://doi.org/10.1021/jacs.5c02540
J. Am. Chem. Soc. 2025, 147, 20504−20511

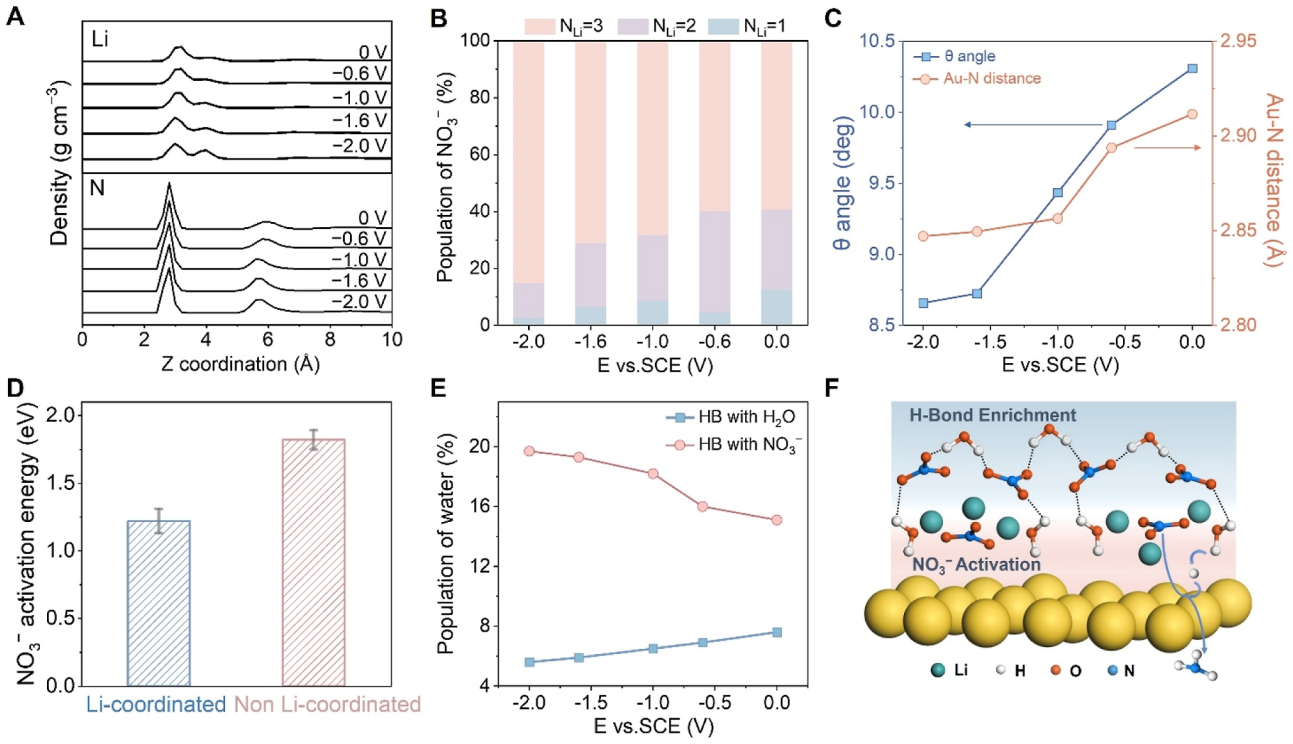

Figure 3. Atomic insights of the EDL at the 1:11 Au(111)/$LiNO_3$ interface. (A) Lithium and nitrogen density profiles normal to the Au(111) surface in the *z*-direction, where zero corresponds to the surface. (B) Population of NO_3^- in the first peak with 1, 2, and 3 lithium coordination numbers. (C) Average angle between the normal direction of the nitrate plane and the normal direction of the Au(111) surface and the average distance of N in the first layer. (D) The activation energy for NO_3^- dissociation with Li-coordinated oxygen and non-Li^+ coordinated oxygen calculated by the slow growth method. (E) The ratio of $H_2O_{N=2}$ for which 2 acceptors are provided entirely by H_2O and for which NO_3^- participates in providing the acceptor. (F) Atomic scheme of the 1:11 Au(111)/$LiNO_3$ interface. Except for panel (D), which is obtained from ab initio molecular dynamics (AIMD) simulations, all other data are generated using constant-potential classical MD, as detailed in the Supporting Information.

information available in the Supporting Information. Raman spectra for Au(111) in 1:11 $LiNO_3$ electrolytes are captured in Figure S6, with the O−H stretching vibration of interfacial of water depicted in Figure 2A. The broad peak from 3520 cm^{-1} to 3300 cm^{-1} is attributed to the O−H stretching vibration of interfacial water. Through a combined approach employing Gaussian fitting methodology and theoretical simulations (Figures S18−S23), we identified three distinct components within the O−H stretching band of interfacial water based on the donor number of hydrogen bonds,[20] specifically, H_2O with 2 donors ($H_2O_{N=2}$) around 3200−3300 cm^{-1}, H_2O with 1 donor ($H_2O_{N=1}$) around 3300−3500 cm^{-1}, and H_2O without any donor ($H_2O_{N=0}$) above 3500 cm^{-1}. The potential-dependent proportion change of each component is quantified and illustrated in Figure 2B by columns. Notably, the population of $H_2O_{N=2}$ and $H_2O_{N=0}$ increases evidently with the negative going potential, while that of $H_2O_{N=1}$ decreases, consistent with the results of classical molecular dynamics simulations, as indicated by the dotted lines.

The observed increase in $H_2O_{N=0}$, predominantly comprised cation-coordinated water ($Li^+{\cdot}H_2O$), which could be attributed to the electrostatic attraction exerted by the negatively charged electrode.[21] Intriguingly, the rise in the $H_2O_{N=2}$ population contradicts the conventional cation-dominated paradigm, where accumulated cations at negative potentials typically disrupt the hydrogen-bond network, leading to a more structured interfacial water layer. The anomalous rise in $H_2O_{N=2}$ may stem from the interactions between H_2O and NO_3^-, which is influenced by the hydrogen bond affinity of NO_3^-. In situ Raman experiments conducted with 1:11 $LiClO_4$ (Figure S7) and LiCl (Figure S8) further support this interpretation, as evidenced by the decrease of $H_2O_{N=2}$ with increasingly negative potentials. These differences arise from the structural diversity of anions and their varied interactions with H_2O. The NO_3^- can be safely regarded as hydrophilic, whereas ClO_4^- and Cl^- own slightly hydrophobic nature, as confirmed by previous studies.[22,23] The observed increase in $H_2O_{N=2}$ populations at negative potentials arises from the unique dual role of NO_3^- as a hydrogen-bond acceptor and a structural linker. This anomaly reflects nitrate's ability to form $Li^+-NO_3^--H_2O$ coordination clusters under interfacial electric fields, which reorganize water networks into dense H-bonded configurations. The involvement of NO_3^- in the EDL significantly alters the characteristics of the interfacial hydrogen-bond networks, which also triggers its own electrochemical conversion.

To further investigate the electrochemical behavior, linear sweep voltammetry (LSV) experiments were carried out in 1:11 $LiNO_3$, $NaNO_3$, and $NaClO_4$ electrolytes. The results showed an early onset potential and an increase in the reduction current, indicating the presence of an additional reduction process in the NO_3^--containing electrolytes (Figure S2A). Gas chromatography (GC) measurements were subsequently utilized (Figures 2C and S14) to evaluate the NO_3RR.[24] The formation of nitrite (NO_2^-) results directly from the detachment of oxygen from NO_3^-, whereas NH_3 represents a product of an eight-electron reduction. As presented in Figure 2C, the NO_2- and NH_3 yield rates

https://doi.org/10.1021/jacs.5c02540
J. Am. Chem. Soc. 2025, 147, 20504−20511

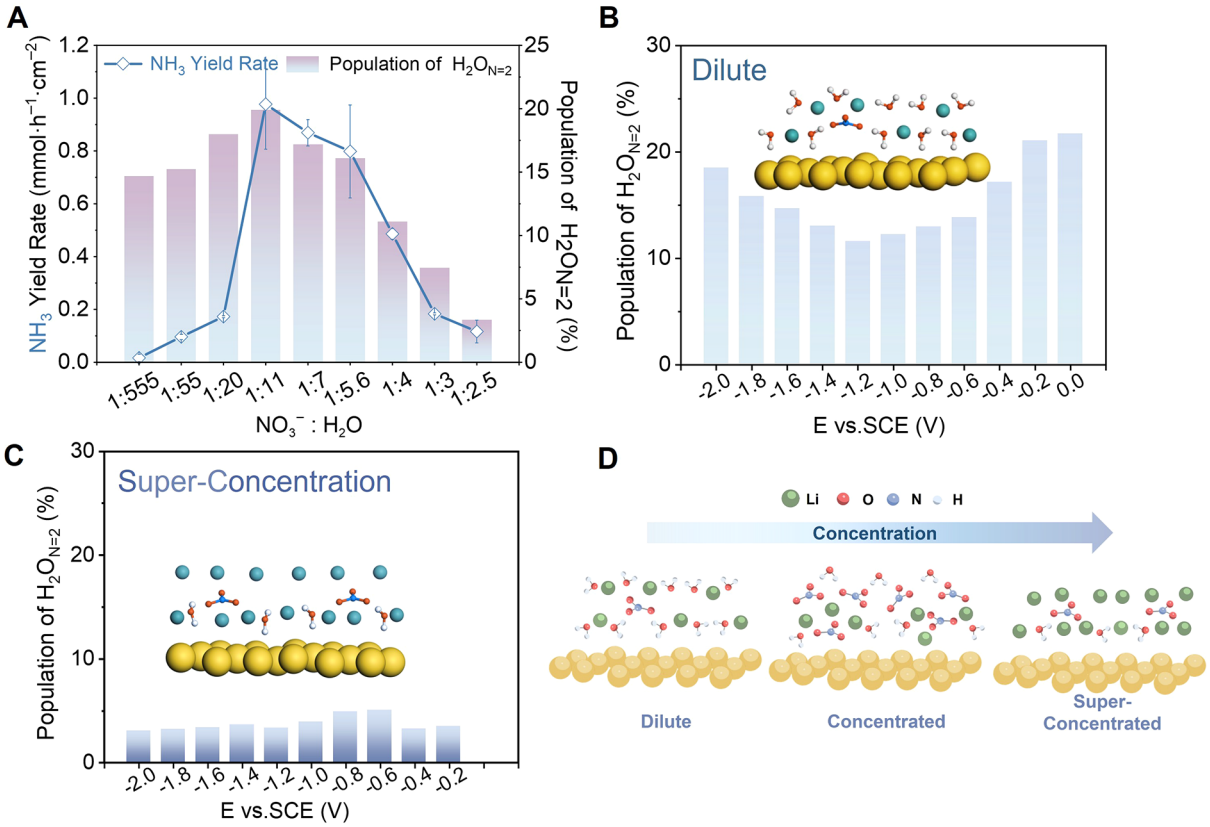

Figure 4. Nitrate reduction and $H_2O_{N=2}$ population. (A) Potential-dependent population of the $H_2O_{N=2}$ (column) and ammonia (blue) yield rate on Au(111) with different $LiNO_3$ concentrations at −1.6 V. (B) Potential-dependent population of $H_2O_{N=2}$ at 1:555 Au(111)/$LiNO_3$ and atomic scheme. (C) Potential-dependent population of $H_2O_{N=2}$ at 1:2.5 Au(111)/$LiNO_3$ and atomic scheme. (D) Schematic diagram of the interfacial aggregation state of water−ion networks in varying concentrations of $LiNO_3$.

escalate as the potential gets negative, correlating with the proportion change of $H_2O_{N=2}$. This observation further indicates that the conversion of NO_3^- to NO_2^- constitutes the rate-determining step in synthesizing NH_3 from NO_3^- on transition metals, consistent with prior studies.[25]

Atomic Insights of EDL Structures. Multifidelity MD simulations were employed to further rationalize the atomic-level structure of the EDL structure at the 1:11 Au(111)/$LiNO_3$ interface (Figure S18). The lithium density profile (Figure 3A) reveals a pronounced enrichment of Li^+ as the potential becomes more negative. Remarkably, NO_3^- demonstrates a pronounced double-peak distribution close to the surface (Figure 3A). The complex interplay of forces from negatively charged Au and accumulated Li^+ contributes to the constant intensity of NO_3^- closest to the interface and they are predominantly coordinated with three Li^+ ions (Figure 3B). The $3Li{\cdot}NO_3^-$ planes are nearly parallel to the interface, as evidenced by calculated angles between the normal NO_3^- plane and the Au(111) interface (Figure 3C). The N atom in $3Li^+{\cdot}NO_3^-$ of the first peak is positioned closer to the interface (Figures 3B and S28), facilitating charge exchange with the electrode. Furthermore, the coordination of Li^+ with the oxygen of NO_3^- results in elongation of the N−O bond (Figure S29), thereby promoting the activation of NO_3^- ($*NO_3 \rightarrow *NO_2 + O*$). The slow growth method was applied to quantificationally calculate the activation ability of oxygen in NO_3^- (Figure 3D), revealing that Li^+ coordination significantly lowers the activation energy of oxygen.[26] Thus, the $3Li^+{\cdot}NO_3^-$ complex exhibits the highest activity due to the coordination of its three oxygen atoms with Li^+.

Regarding the second peak associated with NO_3^- anions, its intensity is observed to increase as the potential shifts negative. This enhancement is attributed to the predominance of the attractive force exerted by lithium ions on NO_3^-, which adopts a configuration that is more perpendicular to the interface (Figure S26) and exhibits reduced interaction with Li^+ (Figure S27). Consequently, the intensification of NO_3^- in the second layer is responsible for the growing population of $H_2O_{N=2}$, owing to the inherent capacity of unbound NO_3^- to serve as a hydrogen-bond acceptors. For further confirmation, we quantified the instances of NO_3^- as hydrogen-bonds acceptors (Figure 3E), and the analysis indicated that more hydrogen bonds of $H_2O_{N=2}$ were associated with NO_3^- as the potential decreased (Figure S25). The strengthened connectivity of the hydrogen-bond networks facilitates proton transfer to the interface,[27,28] which is essential for the conversion of $*NO_2$ to ammonia via proton-coupled electron transfer steps. Figure 3F encapsulates the atomic bilayer EDL structure at the 1:11 Au(111)/$LiNO_3$ interface, illustrating both the NO_3^- activation process and hydrogen bond enrichment. In this scenario, the nitrite yield rate and the population of $H_2O_{N=2}$ are proposed to mirror the ammonia yield rate. Moreover, the $H_2O_{N=2}$ population serves not only as a direct indicator of the EDL structure but also as a predictive descriptor of the NO_3RR activity.

Concentration-Dependent EDL Evolution. The correlations between the $H_2O_{N=2}$ population and the nitrate

https://doi.org/10.1021/jacs.5c02540
J. Am. Chem. Soc. 2025, 147, 20504−20511

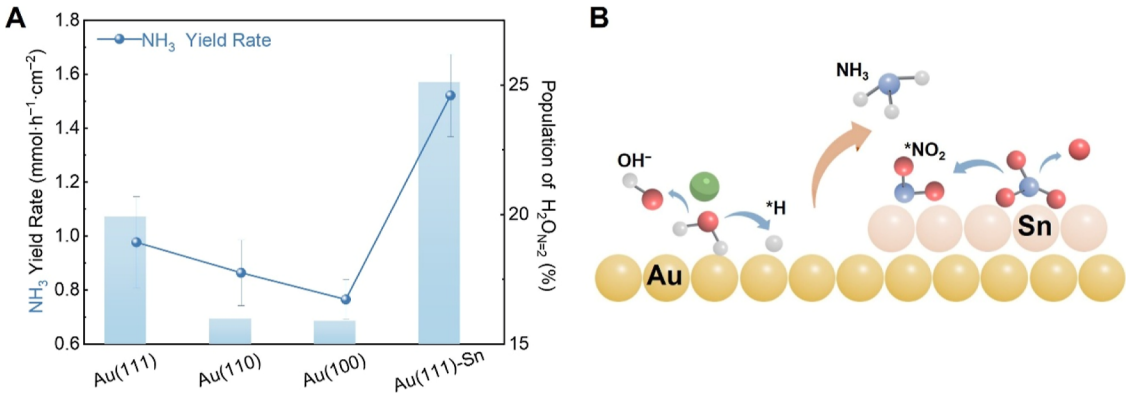

Figure 5. Nitrate reduction at Au(hkl) and Au(111)-Sn interfaces. (A) Potential-dependent NH_3 yield rate and population of $H_2O_{N=2}$ at − 1.6 V at 1:11 Au(111), Au(110), Au(100), and Au(111)-Sn/$LiNO_3$. (B) Schematic diagram of the NO_3RR process at the Au(111)-Sn interface.

reduction activity were further investigated under varied $LiNO_3$ concentrations. Notably, the $H_2O_{N=2}$ population and yield rates of the products exhibited a volcanic-like dependence on concentration with a maximum of 1:11 $LiNO_3$ (Figures 4A and S15). The interplay between NO_3^- and interfacial hydrogen-bond networks, alongside the reduction behavior, underscores a distinct structure−function relationship within the EDL.

Variations in the $H_2O_{N=2}$ population with bias potential were analyzed in both diluted and superconcentrated solutions, as illustrated in Figure 4B,C, respectively. In diluted electrolytes, the limited availability of $LiNO_3$ in the bulk solution restricts the presence of both Li^+ and NO_3^- at the interface. This scarcity results in a more inclined configuration to interact with H_2O at relatively positive potentials (Figure S31), thereby impeding the activation of NO_3^-. Concurrently, although unbound NO_3^- can enhance the hydrogen-bond network of interfacial water, the Li^+ ions dominate the hydrogen-bond networks due to their propensity to aggregate near the interface (inset in Figure 4B). Consequently, this results in a decreasing trend in $H_2O_{N=2}$ at less negative potentials. In contrast, at a highly negative potential, the electric field draws an abundance of Li^+ and NO_3^- to the interface, facilitating the formation of a distinct NO_3^- bilayer. This leads to an increase in the $H_2O_{N=2}$ population, thus boosting the NO_3RR efficiency. In more concentrated electrolyte solutions, a less negative potential is required to organize the NO_3^- bilayer and more $H_2O_{N=2}$ is formed correspondently, correlating with enhanced efficiency in NO_3RR.

However, at excessively high concentrations, a significant decrease in the number of water molecules was observed alongside a considerable enrichment of Li^+ ions at the interface. This leads to the phenomenon that nearly all of the oxygen atoms of interfacial NO_3^- are coordinated with Li^+, rendering them incapable of forming hydrogen bonds with water molecules (the insets are shown in Figures 4C and S32). The weak interaction between the NO_3^- and water molecules results in less connected hydrogen-bond networks within the EDL. In the context of superconcentrated $LiNO_3$, which exhibits a polymer-like structure (Figure S4),[19] the formation of stable $(Li^+(H_2O)_2)_n$ chain maintains a constant population of $H_2O_{N=2}$ population, with minimal variation with changes in potential. The reduction of NO_3^- is thus impeded in superconcentrated Au(111)/$LiNO_3$ on account of structural obstacles and a scarcity of available H_2O. A schematic of the concentration-dependent interfacial solvation structure on Au(111)/$LiNO_3$ is shown in Figure 4D.

The crystallographic orientation and electronic structure of the electrode significantly impact the interfacial water−ion networks. We further monitored the NO_3RR efficiency by tuning the water−ion network through varying the crystallographic orientations of Au single-crystal surfaces (Figures S10, S11). The product (Figures 5A and S16) yield rates follow the order Au(111) > Au(110) > Au(100), sharing a similar trend with the corresponding $H_2O_{N=2}$ population. The more positive point of zero charge (PZC) indicates a higher surface charge density on the Au(111) surface, thereby facilitating the organization of the interfacial bilayer structure.[29] The surface structure thus directly impacts the formation of an efficient EDL, highlighting the critical role of crystallographic orientation in the design of electrocatalytic interfaces.

Building on these findings, we designed a heterostructure by spontaneously adsorbing Sn onto the Au(111) surface to further enhance the nitrate reduction activity. The Au(111)-Sn demonstrated superior NH_3 and NO_2^- yield rate (Figures 5A, S2B, S16 and S17), alongside the highest proportion of $H_2O_{N=2}$ (Figure S12), which could be attributed to the suppression of the competing HER by Sn.[30] The heterostructure design of Au(111)-Sn underscores the importance of combining different materials to leverage synergistic effects, where Sn acts to optimize the interfacial water−ion networks and further enhances the catalytic performance (shown in Figure 5B). The activation energy for dissociation of NO_3^- with Li-coordinated oxygen on Au(111)-Sn was calculated by AIMD (Figure S33). The activation energy decreases to 0.96 eV on Au(111)-Sn, revealing Sn-induced electron redistribution facilitates nitrate adsorption and activation. These findings indicate that the EDL structures share similarities at these electrodes, and the variance in the electrocatalytic performance is primarily derived from the efficiency in orchestrating the bilayer structure, as evidenced by $H_2O_{N=2}$ populations.

CONCLUSIONS

Utilizing Au(*hkl*)/$LiNO_3$ interfaces as a model system, we established a comprehensive framework that deciphers the intricate relationship among interfacial water−ion networks, electrolyte concentration, and nitrate reduction kinetics. At operational potentials, we observed the formation of a hierarchical structure consisting of well-organized cation−anion planes and highly connected hydrogen-bond networks.

https://doi.org/10.1021/jacs.5c02540
J. Am. Chem. Soc. 2025, 147, 20504−20511

The structured cation−anion planes act as a catalyst, driving the attraction and activation of anions through electrostatic forces, while the interconnected hydrogen-bond networks facilitate continuous anion reduction. The efficiency of these interfacial water−ion networks is crucial for constructing the bilayer structure, revealing a volcanic-like relationship between anion reduction efficiency and electrolyte concentration. This insight highlights the intricate interactions between ions and solvents at the interface, which significantly enhance the reduction dynamics of anions. Our findings underscore the critical role of the interfacial water−ion microstructure in optimizing electrocatalytic kinetics, offering valuable guidance for the design and engineering of more efficient and sustainable energy systems.

■ ASSOCIATED CONTENT

Supporting Information

The Supporting Information is available free of charge at https://pubs.acs.org/doi/10.1021/jacs.5c02540.

Detailed methods (synthesis, characterizations, electrochemical measurements, and theoretical calculations) (PDF)

■ AUTHOR INFORMATION

Corresponding Authors

Feng Pan − *School of Advanced Materials, Peking University, Shenzhen Graduate School, Shenzhen 518055, China;* orcid.org/0000-0002-8216-1339; Email: panfeng@pkusz.edu.cn

Jian-Feng Li − *State Key Laboratory of Physical Chemistry of Solid Surfaces, iChEM, College of Chemistry and Chemical Engineering, College of Energy, College of Materials, School of Life Sciences, Xiamen University, Xiamen 361005, China; Fujian Provincial Key Laboratory of Pollution Monitoring and Control, College of Chemistry, Chemical Engineering and Environment, Minnan Normal University, Zhangzhou 363000, China; Innovation Laboratory for Sciences and Technologies of Energy Materials of Fujian Province (IKKEM), Xiamen 361005, China; Liaoning Binhai Laboratory, Liaoning 115004, China;* orcid.org/0000-0003-1598-6856; Email: li@xmu.edu.cn

Authors

Ru-Yu Zhou − *State Key Laboratory of Physical Chemistry of Solid Surfaces, iChEM, College of Chemistry and Chemical Engineering, College of Energy, College of Materials, School of Life Sciences, Xiamen University, Xiamen 361005, China*

Shisheng Zheng − *State Key Laboratory of Physical Chemistry of Solid Surfaces, iChEM, College of Chemistry and Chemical Engineering, College of Energy, College of Materials, School of Life Sciences, Xiamen University, Xiamen 361005, China; School of Advanced Materials, Peking University, Shenzhen Graduate School, Shenzhen 518055, China;* orcid.org/0009-0000-4529-7440

Xuan Liu − *State Key Laboratory of Physical Chemistry of Solid Surfaces, iChEM, College of Chemistry and Chemical Engineering, College of Energy, College of Materials, School of Life Sciences, Xiamen University, Xiamen 361005, China*

Yao-Hui Wang − *State Key Laboratory of Physical Chemistry of Solid Surfaces, iChEM, College of Chemistry and Chemical Engineering, College of Energy, College of Materials, School of Life Sciences, Xiamen University, Xiamen 361005, China*

Shunning Li − *School of Advanced Materials, Peking University, Shenzhen Graduate School, Shenzhen 518055, China;* orcid.org/0000-0002-5381-6025

Xinzhe Yang − *School of Advanced Materials, Peking University, Shenzhen Graduate School, Shenzhen 518055, China;* orcid.org/0009-0008-1921-0629

Complete contact information is available at: https://pubs.acs.org/10.1021/jacs.5c02540

Author Contributions

#R.-Y.Z. and S.Z. contributed equally.

Notes

The authors declare no competing financial interest.

■ ACKNOWLEDGMENTS

This work was supported by grants from the National Natural Science Foundation of China (22525042, T2293692, 22021001, 22322206, 22361132532, and 22402163), the State Key Laboratory of Fine Chemicals, Dalian University of Technology (KF 2401), NFFTBS (No. J1310024), the Liaoning Binhai Laboratory (Grant No. 2024-05), the New Cornerstone Science Foundation through the XPLORER PRIZE, Soft Science Research Project of Guangdong Province (2017B030301013), and the Major Science and Technology Infrastructure Project of Material Genome Big-science Facilities Platform supported by the Municipal Development and Reform Commission of Shenzhen, Shenzhen Science, and Technology Research Grant (ZDSYS201707281026184).

■ REFERENCES

(1) Guo, J.; Chen, P. Catalyst NH_3 as an energy carrier. *Chem.* **2017**, *3* (5), 709−712.

(2) van Langevelde, P. H.; Katsounaros, I.; Koper, M. T. M. Electrocatalytic nitrate reduction for sustainable ammonia production. *Joule* **2021**, *5* (2), 290−294.

(3) Liang, J.; Li, Z.; Zhang, L.; He, X.; Luo, Y.; Zheng, D.; Wang, Y.; Li, T.; Yan, H.; Ying, B.; Sun, S.; Liu, Q.; Hamdy, M. S.; Tang, B.; Sun, X. Advances in ammonia electrosynthesis from ambient nitrate/nitrite reduction. *Chem.* **2023**, *9*, 1768−1827.

(4) Zheng, S.; Yang, X.; Shi, Z.-Z.; Ding, H.; Pan, F.; Li, J.-F. The loss of interfacial water-adsorbate hydrogen bond connectivity position surface-active hydrogen as a crucial intermediate to enhance nitrate reduction reaction. *J. Am. Chem. Soc.* **2024**, *146*, 26965−26974.

(5) Zhang, L.; Hu, H.; Sun, C.; Xiao, D.; Wang, H.-T.; Xiao, Y.; Zhao, S.; Chen, K. H.; Lin, W.-X.; Shao, Y.-C.; Wang, X.; Pao, C.-W.; Han, L. Bimetallic nanoalloys planted on super-hydrophilic carbon nanocages featuring tip-intensified hydrogen evolution electrocatalysis. *Nat. Commun.* **2024**, *15* (1), 7179.

(6) Li, S.; Wu, L.; Liu, Q.; Zhu, M.; Li, Z.; Wang, C.; Jiang, X.; Li, J. Uncovering the dominant role of an extended asymmetric four-coordinated water network in the hydrogen evolution reaction. *J. Am. Chem. Soc.* **2023**, *145* (49), 26711−26719.

(7) Li, P.; Jiang, Y.; Hu, Y.; Men, Y.; Liu, Y.; Cai, W.; Chen, S. Hydrogen bond network connectivity in the electric double layer dominates the kinetic pH effect in hydrogen electrocatalysis on Pt. *Nat. Catal.* **2022**, *5* (10), 900−911.

(8) Wang, Y.-H.; Zheng, S.; Yang, W.-M.; Zhou, R.-Y.; He, Q. F.; Radjenovic, P.; Dong, J.-C.; Li, S.; Zheng, J.; Yang, Z.-L.; Attard, G.; Pan, F.; Tian, Z.-Q.; Li, J.-F. In situ Raman spectroscopy reveals the structure and dissociation of interfacial water. *Nature* **2021**, *600* (7887), 81−85.

(9) Gomez, A.; Thompson, W. H.; Laage, D. Neural-network-based molecular dynamics simulations reveal that proton transport in water

is doubly gated by sequential hydrogen-bond exchange. *Nat. Chem.* **2024**, *16*, 1838−1844.
(10) Chen, X.; Cheng, Y.; Zhang, B.; Zhou, J.; He, S. Gradient-concentration RuCo electrocatalyst for efficient and stable electroreduction of nitrate into ammonia. *Nat. Commun.* **2024**, *15* (1), 6278.
(11) Liu, Y.; Wei, J.; Yang, Z.; Zheng, L.; Zhao, J.; Song, Z.; Zhou, Y.; Cheng, J.; Meng, J.; Geng, Z.; Zeng, J. Efficient tandem electroreduction of nitrate into ammonia through coupling Cu single atoms with adjacent Co_3O_4. *Nat. Commun.* **2024**, *15* (1), 3619.
(12) Zhang, Z.-M.; Wang, T.; Cai, Y.-C.; Li, X.-Y.; Ye, J.-Y.; Zhou, Y.; Tian, N.; Zhou, Z.-Y.; Sun, S.-G. Probing electrolyte effects on cation-enhanced CO_2 reduction on copper in acidic media. *Nat. Catal.* **2024**, *7*, 807−817.
(13) Tian, Y.; Huang, B.; Song, Y.; Zhang, Y.; Guan, D.; Hong, J.; Cao, D.; Wang, E.; Xu, L.; Shao-Horn, Y.; Jiang, Y. Effect of ion-specific water structures at metal surfaces on hydrogen production. *Nat. Commun.* **2024**, *15* (1), 7834.
(14) Yamada, Y.; Wang, J.; Ko, S.; Watanabe, E.; Yamada, A. Advances and issues in developing salt-concentrated battery electrolytes. *Nat. Energy* **2019**, *4* (4), 269−280.
(15) Borodin, O.; Self, J.; Persson, K. A.; Wang, C.; Xu, K. Uncharted waters: super-concentrated electrolytes. *Joule* **2020**, *4* (1), 69−100.
(16) Wang, Y.; Wang, Z.; Pang, W. K.; Lie, W.; Yuwono, J. A.; Liang, G.; Liu, S.; Angelo, A. M. D.; Deng, J.; Fan, Y.; Davey, K.; Li, B.; Guo, Z. Solvent control of water O-H bonds for highly reversible zinc ion batteries. *Nat. Commun.* **2023**, *14*, 2720.
(17) Li, J.-F.; Huang, Y.-F.; Ding, Y.; Yang, Z.-L.; Li, S. B.; Zhou, X.-S.; Fan, F. R.; Zhang, W.; Zhou, Z.-Y.; Wu, D.-Y.; Ren, B.; Wang, Z.-L.; Tian, Z.-Q. Shell-isolated nanoparticle-enhanced Raman spectroscopy. *Nature* **2010**, *464* (7287), 392−395.
(18) Li, C.-Y.; Le, J.-B.; Wang, Y.-H.; Chen, S.; Yang, Z.-L.; Li, J.-F.; Cheng, J.; Tian, Z.-Q. In situ probing electrified interfacial water structures at atomically flat surfaces. *Nat. Mater.* **2019**, *18* (7), 697−701.
(19) Zheng, J.; Tan, G.; Shan, P.; Liu, T.; Hu, J.; Feng, Y.; Yang, L.; Zhang, M.; Chen, Z.; Lin, Y.; Lu, J.; Neuefeind, J. C.; Ren, Y.; Amine, K.; Wang, L.-W.; Xu, K.; Pan, F. Understanding thermodynamic and kinetic contributions in expanding the stability window of aqueous electrolytes. *Chem.* **2018**, *4* (12), 2872−2882.
(20) Chen, X.; Wang, X.-T.; Le, J.-B.; Li, S.-M.; Wang, X.; Zhang, Y.-J.; Radjenovic, P.; Zhao, Y.; Wang, Y.-H.; Lin, X.-M.; Dong, J.-C.; Li, J.-F. Revealing the role of interfacial water and key intermediates at ruthenium surfaces in the alkaline hydrogen evolution reaction. *Nat. Commun.* **2023**, *14*, 5289.
(21) Wang, Y.-H.; Jin, X.; Xue, M.; Cao, M.-F.; Xu, F.; Lin, G.-X.; Le, J.-B.; Yang, W.-M.; Yang, Z.-L.; Cao, Y.; Zhou, Y.; Cai, W.; Zhang, Z.; Cheng, J.; Guo, W.; Li, J.-F. Characterizing surface-confined interfacial water at graphene surface by in situ Raman spectroscopy. *Joule* **2023**, *7* (7), 1652−1662.
(22) Zhang, H.; Gao, J.; Raciti, D.; Hall, A. S. Promoting Cu-catalysed CO_2 electroreduction to multicarbon products by tuning the activity of H_2O. *Nat. Catal.* **2023**, *6*, 807−817.
(23) Tong, Y.; Zhang, I. Y.; Campen, R. K. Experimentally quantifying anion polarizability at the air/water interface. *Nat. Commun.* **2018**, *9*, 1313.
(24) Hao, J.; Wang, T.; Yu, R.; Cai, J.; Gao, G.; Zhuang, Z.; Kang, Q.; Lu, S.; Liu, Z.; Wu, J.; Wu, G.; Du, M.; Wang, D.; Zhu, H. Integrating few-atom layer metal on high-entropy alloys to catalyze nitrate reduction in tandem. *Nat. Commun.* **2024**, *15* (1), 9020.
(25) Yin, H.; Chen, Z.; Xiong, S.; Chen, J.; Wang, C.; Wang, R.; Kuwahara, Y.; Luo, J.; Yamashita, H.; Peng, Y.; Li, J. Alloying effect-induced electron polarization drives nitrate electroreduction to ammonia. *Chem Catal.* **2021**, *1* (5), 1088−1103.
(26) Woo, T. K.; Margl, P. M.; Blochl, P. E.; Ziegler, T. A Combined Car-Parrinello QM/MM Implementation for ab Initio Molecular dynamics simulations of extended systems: application to transition metal catalysis. *J. Phys. Chem. B* **1997**, *101* (40), 7877−7880.
(27) Mohammed, O. F.; Pines, D.; Dreyer, J.; Pines, E.; Nibbering, E. T. J. Sequential proton transfer through water bridges in acid-Base reactions. *Science* **2005**, *310*, 83−86.
(28) Wolke, C. T.; Fournier, J. A.; Dzugan, L. C.; Fagiani, M. R.; Odbadrakh, T. T.; Knorke, H.; Jordan, K. D.; McCoy, A. B.; Asmis, K. R.; Johnson, M. A. Spectroscopic snapshots of the proton-transfer mechanism in water. *Science* **2016**, *354* (6316), 1131−1135.
(29) Kim, M.; Batsa Tetteh, E.; Krysiak, O. A.; Savan, A.; Xiao, B.; Piotrowiak, T. H.; Andronescu, C.; Ludwig, A.; Dong Chung, T.; Schuhmann, W. Acidic hydrogen evolution electrocatalysis at high-entropy alloys correlates with its composition-dependent potential of zero charge. *Angew. Chem., Int. Ed.* **2023**, *62* (39), No. e202310069.
(30) Shao, J.; Jing, H.; Wei, P.; Fu, X.; Pang, L.; Song, Y.; Ye, K.; Li, M.; Jiang, L.; Ma, J.; Li, R.; Si, R.; Peng, Z.; Wang, G.; Xiao, J. Electrochemical synthesis of ammonia from nitric oxide using a copper-tin alloy catalyst. *Nat. Energy* **2023**, *8* (11), 1273−1283.

https://doi.org/10.1021/jacs.5c02540
J. Am. Chem. Soc. 2025, 147, 20504−20511